The International Journal of Advanced Manufacturing Technology (2018) 99:1877–1889
https://doi.org/10.1007/s00170-018-2605-6

ORIGINAL ARTICLE

A convective heat transfer coefficient algorithm for thermal analysis of machine tools considering a temperature change

Xiaobo Mao[1] · Kuanmin Mao[1] · Fengyun Wang[1] · Bo Yan[1] · Sheng Lei[2]

Received: 2 May 2018 / Accepted: 15 August 2018 / Published online: 28 August 2018

Abstract
The convective heat transfer coefficient (CHTC) is a key parameter for thermal analysis. The calculation method of empirical equations cannot accurately reflect the real situation of an object, especially when the fluid temperature is a variable, making the CHTC calculation more difficult. Based on finite element (FE) thermal analysis, an iterative algorithm of FE thermal analysis combined with experimental data was proposed. Furthermore, in the thermal analysis process, the temperature of the object itself changes and the heat is not uniform. The adopted CHTCs dynamically varied with the uneven wall temperature and ambient temperature. A CHTC gradual change "dynamic boundary condition" application mode was used. The interactive iterative calculation was completed by the FE software ABAQUS 6.14 and MATLAB 2016b, and a program was written to improve the calculation accuracy of the CHTC using multiple iterations. Taking the machine tool ball screw feed system as an example, a large number of experiments were conducted over 1 year under different ambient temperatures to verify that the method described in this paper was accurate and feasible. In addition, the relationship between the CHTC and ambient temperature change was found determined, and an explanation was provided.

Keywords Convective heat transfer coefficient (CHTC) · Thermal analysis · Ball screw feed system · FE simulation

1 Introduction

The presence of thermal errors in machine tools is increasing and can occur in up to 40–70% of tools [1, 2], demonstrating the urgent need for methods to reduce these errors. Thermal analysis is widely used as an effective method to reduce thermal error [3–5]. However, the accuracy of this method is affected by the precision of the temperature field distribution model, which has become a very critical part of tool design and development [6, 7]. Two methods can be used to establish the temperature field model, experimental measurements and FE simulations. Compared with the FE method, the experimental method is more accurate but may be limited by the experimental conditions. Temperature measurement points often cannot cover the whole machine tool; therefore, the information of the entire machine cannot be obtained. Thus, the current method for establishing an overall machine tool temperature field is an FE simulation calculation, and the experimental measurement method is used to verify the accuracy of the simulation results. However, in the FE method, it is difficult to set the boundary condition of the thermal analysis, and the process is typically not consistent with actual situations [8], thus increasing thermal analysis errors [9].

The most common calculation method of CHTC is based on similarity criteria; however, the similarity criteria are closely related to or influenced by the experiment, conditions and various other factors. Hence, the calculated results also deviate. Yang et al. [10] presented a method to combine experimental data and an RBF neural network to calculate the CHTC of a ball screw. Li et al. [11] constructed a neural network based on RBF to compute the CHTC for thermal simulation of a spindle system. Fan [12] presented an inverse method based on thermographic temperature measurements, and the CHTC distribution of a flat plate surface was estimated by iteratively calculating the temperature distribution equations. Zhang et al. [13] proposed a method for thermal performance modelling and simulation of machine tools by considering the simulation boundary conditions, and they studied the

✉ Kuanmin Mao
maokm@hust.edu.cn

[1] School of Mechanical Science and Engineering, Huazhong University of Science and Technology, Wuhan 430074, China

[2] School of Electronic Information Engineering, South-Central University for Nationalities, Wuhan 430074, China

data flow and required initial and boundary conditions for the thermal-structural coupled FE simulation method. Shi et al. [14] adopted an experiment-based thermal error modelling method to study a dual ball screw feed system of precision machine tool. Neugebauer R [15] provided an extended procedure for determining the convective boundary conditions of transient thermal simulations of machine tools to help set boundary conditions for thermal analyses.

In this paper, the CHTC, the key parameter in thermal analysis, was studied in detail, and the CHTC was recalculated and calibrated while taking into account the impact of varying temperature differences in the calculation process. Thus, the boundary condition setting was closer to results in actual situations. In addition, a discrete segment-loading model called the dynamic boundary condition was proposed in the thermal analysis. Finally, the time period of drastic external temperature changes was selected in 1 year. Using a vertical milling centre feed system as an example, the CHTC calculation method presented in this paper was verified, and the relationship between the effects of ambient temperature changes and the CHTC was discussed.

2 CHTC calculation method

2.1 Calculation principle

Currently, the CHTC calculation method is the most commonly used empirical formula, but the method is generally influenced by similar experimental correlations, which have a low calculation accuracy for engineering problems that require high precision [16, 17]. Based on the empirical formula calculation method, which combines FE thermal analysis and experimental data, an iterative CHTC calculation method using FE thermal analysis is presented in this paper.

A small temperature difference Δt was experimentally measured in a very small period of time; then, the CHTCs were calculated using an empirical formula and were then used in thermal analysis to obtain the corresponding temperature field distribution. Then, the temperature field and measured temperature values were compared to determine whether the error between the simulation and experimental values was less than 1% as the judgement condition. Through joint programming with MATLAB and Python, the cycle computation of the above judgement was performed, CHTCs that do not meet the requirement were corrected, and thermal analysis was repeated. Additionally, the CHTC was affected by the temperature difference. In thermal analysis, the temperature difference changes as the temperature of the object increases. Therefore, a constant CHTC in the analysis could inevitably lead to certain errors. The total temperature difference of the research object was divided into several sub-temperature differences, and the CHTCs for each sub-temperature difference were obtained by the calculation method presented in this paper. Then, in thermal analysis, a changed "dynamic CHTC" setting mode was used, which reduced the influence of the temperature difference on the accuracy of the CHTC calculation and improved the simulation precision.

The CHTC was corrected by adding or subtracting one or more Δh from the initial CHTC calculated by the empirical formula. According to the literature [10, 11], in the FE temperature field simulation calculation of a machine tool, the value of CHTC is 3–10 times greater than the theoretical calculation value. Therefore, integers of the CHTC theoretical calculation values were used as the values in the $\triangle$h database. The program was designed to perform a modified and circulation calculation of the CHTC by adding and subtracting Δh when the values did not satisfy the judgement conditions. When addition or subtraction Δh failed to satisfy the judgement condition, the program automatically halved the current Δh value until the condition was satisfied.

2.2 Calculation process

The complete process of the CHTC calculation method at the defined ambient temperature presented in this paper was as follows:

First, the FE thermal analysis model was established. Over a very small period of time, the surface temperature of the object was increased by heat generation; then, temperature $t1$ was measured. According to the ambient temperature $t0$, the corresponding temperature difference $\Delta t1$ was calculated. Then, the CHTC $h1$ was calculated used MATLAB, and $h1$ was used in thermal analysis to find the temperature field T1.

Next, the temperature field T1 and experimentally measured temperature field T0 were compared. When the simulation error of the temperature field was less than 1%, $h1$ was considered to be the exact value. Otherwise, $h1$ needed to be corrected. When (T1-T0)/T0 < 1% was not established, the temperature fields T0 and T1 were judged immediately. If T1 was larger than T0, a Δh was added to $h1$, $h2 = h1 + \Delta h$. Then, $h2$ was used to repeat the thermal analysis. If T1 was less than T0, then a Δh was reduced on the basis of $h1$, $h3 = h1 - \Delta h$. Then, thermal analysis was carried out again with $h3$. The program was designed to achieve a cycle of the above calculation steps until the conditions were satisfied.

Finally, considering CHTC was affected by temperature difference. To better represent the actual situation and improve the simulation accuracy, the thought of FE was applied to divide the total temperature difference into several subintervals. Combined with the temperature values of the experimental measured points, the CHTCs of each subinterval were calculated using the method presented in this paper. After that, in FE thermal analysis, the CHTC was set as a dynamic parameter that changed with temperature. In the simulation calculation process, different CHTCs were called in the

corresponding temperature section, which formed a dynamic CHTC setting mode that changed with temperature. The model was closer to the actual situation and helped to improve the accuracy of the simulation analysis results.

To sum up, the CHTC algorithm process can be summarised into two portions. One was to introduce experimental data to design an algorithm module for accurately calculation single CHTC; the other was the division of the multi temperature difference and the setting of dynamic boundary conditions to solve the temperature field. The algorithm research process of the CHTCs is shown in Fig. 1.

3 CHTC thermal analysis and calculation

3.1 Thermal test of the ball screw feed system

The milling centre ball screw feed system consists of a table, saddle and ball screw. For thermal analysis of the feed system, the following experiment was designed. The feed speed of the table along the X-axis was 4000 mm per minute, and the motor speed was 267 turns per minute. The total experimental time was 4 h. The ambient temperature of the machine tool was approximately 11 °C.

The heat source of the machine tool was relatively fixed. Accordingly, to accurately establish the temperature field of the feed system, some key temperature points [18–20] were chosen, and nine platinum resistance temperature sensors (T1-T9) were fixed on the feed system [21], as shown in Fig. 2. Besides, three platinum resistance temperature sensors were placed in the air around the feed system, and a high precision humidity and temperature meter were placed on the table top to measure the real-time change of the ambient temperature. It can be seen from the multiple sets of measurement data that the ambient temperature changes within the range of 0.2–0.6 °C. Therefore, under the closed workshop ambient temperature, small fluctuation of the ambient temperature has little effect on data acquisition and simulation calculation of the experimental testing system. The experimental testing platform is shown in Fig. 3.

3.2 Establishment of the thermal analysis model

3.2.1 Establishment of the solid model

The solid model of the feed system is shown in Fig. 2, and the ball screw was not established in the solid model since the temperature of the ball screw pair could not be measured directly by the platinum resistance temperature sensor under the current experimental conditions. But in the simulation calculation process, the heat generation of the ball screw pair was taken into consideration. The heat generated from the ball

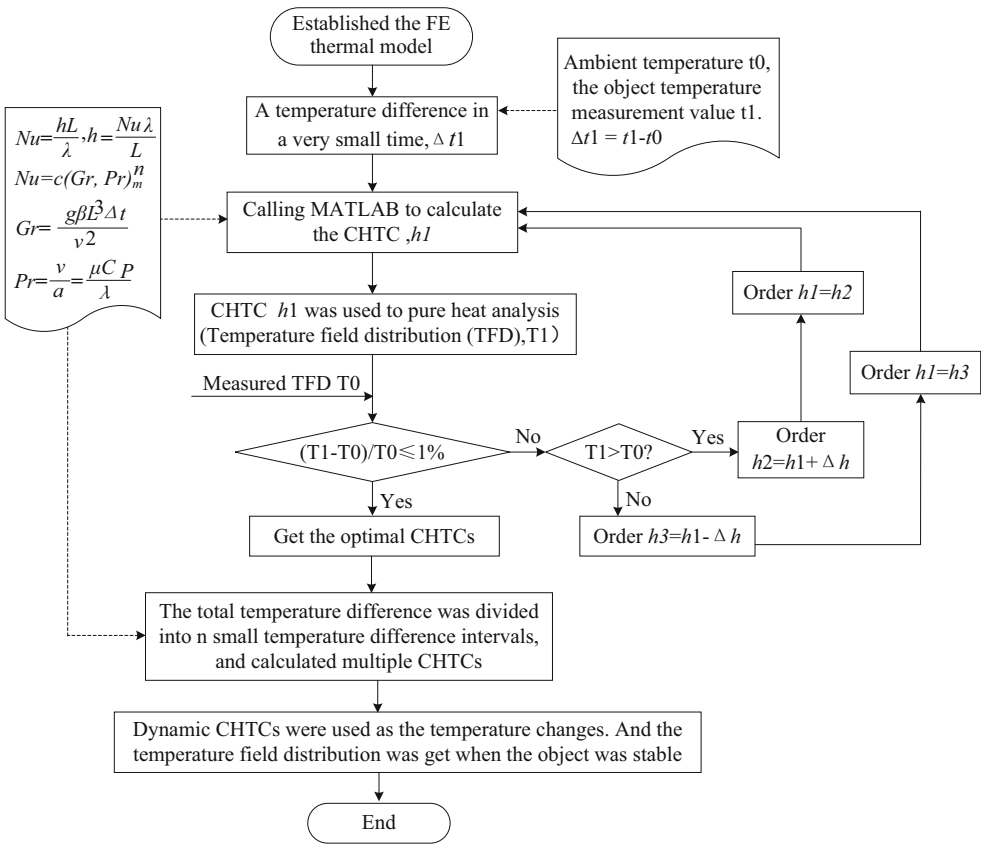

Fig. 1 Algorithm research process of the CHTCs

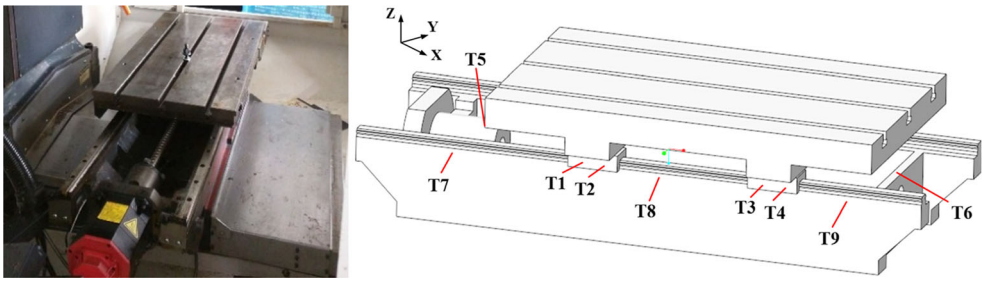

Fig. 2 Ball screw feed system and temperature measuring points

screw pair was loaded on the screw bearings at both ends of the ball screw according to the heat conduction theory and the distance between the ball screw pair and the two ends of the ball screw bearings. Therefore, two temperature sensors (T5 and T6) were fixed near both ends of the ball screw to monitor the temperature changes of the screw, and in the subsequent analysis, the case of no ball screw was considered. Therefore, the results of thermal analysis were not affected in the case of no ball screw in the solid model.

3.2.2 Development of the finite element model

The feed system used two major materials, Uniloy Alloy and HT300. Uniloy Alloy was applied to the guide-ways and slider. Furthermore, the saddle, motor coupling and table used HT300. The properties of the two material were assigned to the respective structures in ABAQUS, and the property values are shown in Table 1. In addition, chamfers, holes and fillets were ignored. In this paper, the four-node linear heat transfer tetrahedron DC3D4 element type and the automatic partitioning method for meshing was adopted to establish the FE model by ABAQUS. When determining the mesh size, the relationship between the displacement precision and the computation time that varies with the mesh quantity was taken into account. The mesh size of the FE model was determined according to the type of data, the condition of loading and grids economic. Moreover, the single guide-way of the machine tool feed system was selected to perform multiple trials of different mesh size, and finally determining the existing grid division was relatively optimal. Figure 4 shows the results with 61,616 elements and 15,951 nodes.

3.3 Thermal source analysis

3.3.1 Heat generation in the motor

Motor heat is a very complex process, so in currently used CNC machine tools, heat generation in the motor is computed by the following equation [22]:

$$H = \frac{M_T n}{9550}(1\text{-}\eta) \tag{1}$$

where M_T is the output torque of the motor (N_{mm}), n is the rotating speed of the motor rpm, and η is the motor efficiency.

3.3.2 Computation of the ball screw bearing friction heat

A single row angular contact bearing was used in the feed system presented in this article. The friction heat generated by these bearings was similar to that of the guide-ways, which can be calculated by the following equation [7, 23, 24]:

$$H_f = 1.047 \times 10^{-4} nM \tag{2}$$

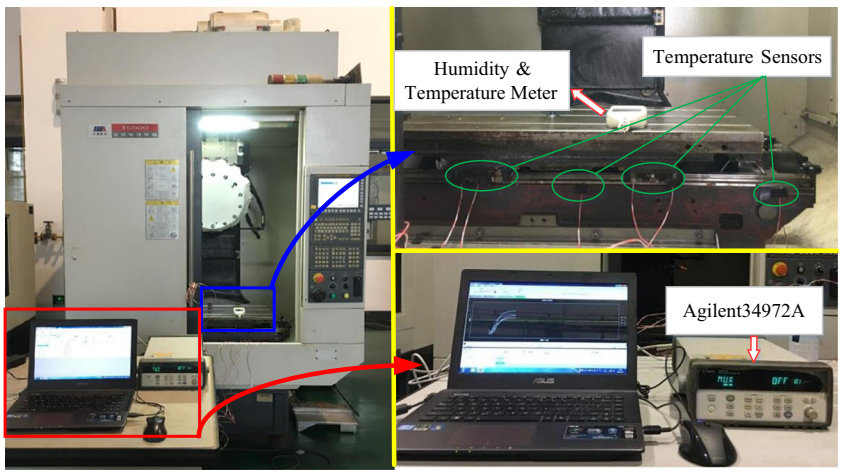

Fig. 3 Experimental testing platform

Table 1 Material properties of the ball screw feed system

Material	Uniloy alloy	HT300
Density (kg m^{-3})	7820	7300
Modulus of elasticity (Gpa)	206	143
Poisson's ratio	0.30	0.27
Linear expansion coefficient (10^{-5} K^{-1})	1.10	1.12
Thermal conductivity (Wm^{-1} K^{-1})	16.3	45
Specific heat capacity (Jkg^{-1} K^{-1})	460	510

where M is the frictional torque of the bearing (Nmm), n is the rotating speed of the bearing (rpm), and H_f is the heat generated power (W). The total frictional torque Mconsists of two parts and can be calculated as follows:

$$M = M_1 + M_2 \tag{3}$$

where M_1 is the mechanical friction torque caused by the applied load, M_2 is the viscous friction torque due to the viscosity of the lubricant.

$$M_1 = f_1 p_1 d_m \tag{4}$$

where f_1 is the factor related to the bearing type and load, p_1 is the bearing preload (N), and d_m is the mean diameter of the bearing (mm).

$$M_2 = 10^{-7} f_0 (v_0 n)^{2/3} d_m \quad if\ v_0 n \geq 2000 \tag{5}$$

$$M_2 = 160 \times 10^{-7} f_0 d_m^3 \quad if\ v_0 n < 2000 \tag{6}$$

where f_0 is the factor related to bearing type and lubrication method and v_0 is the kinematic viscosity of the lubricant.

3.3.3 Computation of the ball screw pair friction heat

The calculation method of friction heat generation of the ball screw pair is the same as that of ball screw bearing, but the friction torque is different. The friction moment can be calculated by the following empirical equation [25]:

$$M = 2z(Me + Mg)\cos\beta \tag{7}$$

where z is the of rolling elements, β is the screw helix angle,Me is the friction resistance moment (Nmm), and Mg is the geometric sliding friction torque (Nmm).where,

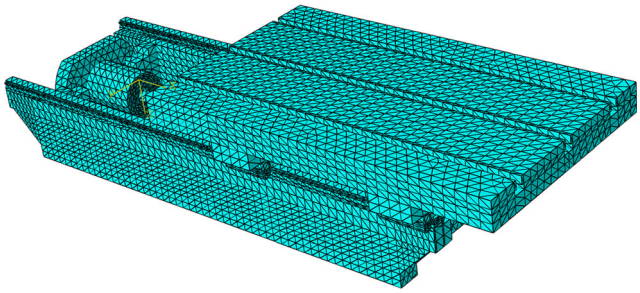

Fig. 4 FE model of the ball screw feed system

Table 2 Heat transfer coefficients of contact surfaces

Type of joint surface	Heat transfer coefficient (W m^{-2} $°C^{-1}$)
Steel joint	3200
Cast iron joint	1800

$$Me = m_\beta \left(\frac{4F}{\nu\sum\rho}\right)^{1/3} \tag{8}$$

$$Mg = 0.08\frac{\mu \cdot m_\alpha^2}{R}\left(\frac{16F^5}{(\nu\sum\rho)^2}\right)^{1/3} \tag{9}$$

$$\nu = \frac{8}{3}\left(\frac{1-\sigma_1^2}{E_1} + \frac{1-\sigma_2^2}{E_2}\right)^{-1} \tag{10}$$

where ν is the sliding velocity, it can be determined by eq. (10). m_α and m_β are the coefficient related to the eccentricity of the sphere contact deformation ellipse. F is radial pressure of a single sphere (N), $\mu$is sliding friction coefficient. σ_1 and σ_2 are the Poisson's ratio of the materials. E_1 and E_2 are the modulus of elasticity (Gpa). $\sum\rho = \rho_{11} + \rho_{12} + \rho_{21} + \rho_{22}$, ρ_{11},ρ_{12},ρ_{21} and ρ_{22} are the principal curvature of two rolling bodies. $R = \frac{R_1 R_2}{R_1 + R_2}$, R_1 and R_2 are the radius of curvature of the raceway and the ball.

With the eqs. (2) (7)–(10), the heat generation of the ball screw pair can be calculated, and then, it is converted into the thermal load applied to both ends of the ball screw bearings through the knowledge of heat conduction.

3.3.4 Computation of the friction heat of the guide-ways

The guide-ways are the HSR25A type, which is a rolling guide. When calculating their friction heat, the friction coefficient must be taken into account, but the friction mode cannot be considered. The friction heat generated can be computed by the following equation:

$$Q = \mu F \nu \tag{11}$$

Table 3 Results of heat flux of the heat sources

Heat source	Heat flux (W m^{-2})
Table slider	2008
Motor cabinet	875
Left slider of the guide-ways	2008
Right slider of the guide-ways	1667
Left ball screw bearing	776
Right ball screw bearing	750

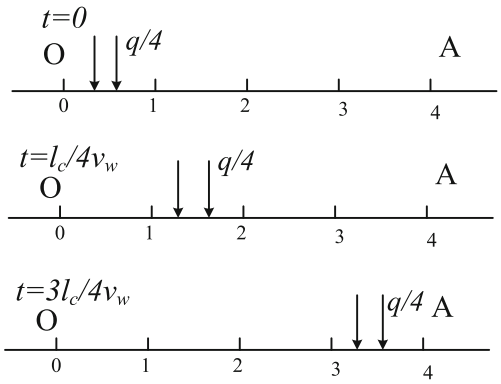

Fig. 5 Loading principle of the mobile heat source

where Q is the generation heat (W), $\mu$is the friction coefficient, F is the pressure applied to the friction surface (N), and ν is the velocity of table (m s^{-1}).

3.3.5 Computation results of the heat flux

The calorific value of each heat source can be calculated according to the heat generation formula. In this study, thermal contact resistances at the main joints affecting thermal transfer in the feed system were considered. The surface heat transfer coefficient is shown in Table 2, which was usually determined by experimental measurements. On the basis of the heat transfer theory and the related knowledge of thermal contact resistance between the bonding parts, the specific heat flux of the heating components was given. And the heat flux of the ball screw pair was transferred to the both ends of the screw bearings. Then, the heat flux was loaded into the FE model in form of thermal load. The calculation results of the heat flux of the heat sources are shown in Table 3.

3.4 CHTC calculation

3.4.1 Moving heat source loading

Using the ball screw feed system of machine tool as an example, the ambient temperature is 11 °C. The friction heat generated by the slider and the guide-ways belongs to a moving heat source, and the moving heat source loading is a very important step in the FE thermal analysis. Currently, the most commonly used method is to use a heat source function to simulate moving heat loading. This method ensures that the boundary condition is set more closely to the actual situation. However, the rapid increase of calculation time and

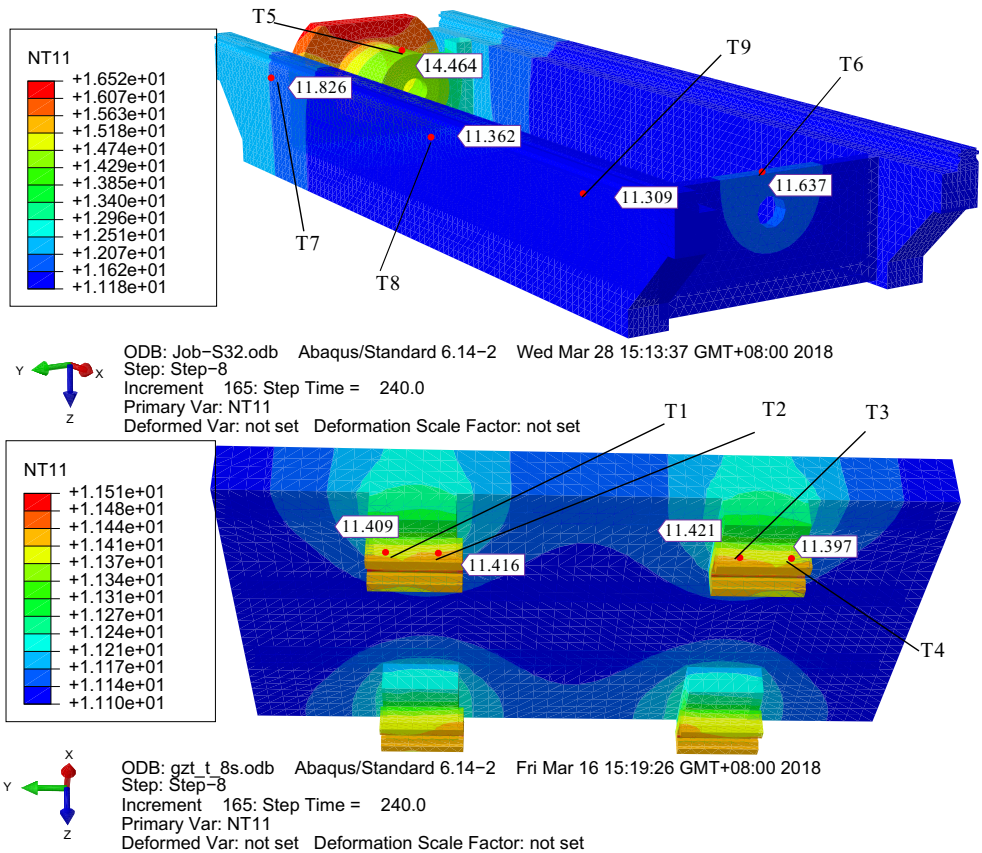

Fig. 6 Exact simulation results in the first 32 min

Table 4 NCHTCs of the plate h_p (W m^{-2} K^{-1})

Ambient temperature	Wall temperature	Temperature difference	NCHTCs (h_p)	
			Theoretical values	Simulation values
11 °C	12 °C	1 °C	1.862	7.448
	13 °C	2 °C	2.213	8.852
	14 °C	3 °C	2.448	9.792
	15 °C	4 °C	2.629	10.516
	16 °C	5 °C	2.779	11.116
	17 °C	6 °C	2.907	11.628
	18 °C	7 °C	3.020	12.080

calculation amount makes the most commonly used loading method not necessarily the best. Moreover, friction heat comes from friction power consumption, so the total friction heat was identical in the contact area regardless of the function distribution of the heat source model used to analyse the friction heat. Therefore, in this paper, a subsection loading method under uniform load is presented. That is, over a very short period of time, a fixed heat flux was loaded into a region of the friction plane. Over the next short time period, the fixed heat flux loading moved to another friction plane. Thus, the moving heat source generated by the friction was able to be loaded on the entire friction plane.

According to the table velocity and data sampling time, each of the guide-ways friction planes was divided into five regions. A slider is used as an example, where section 0 is the length of the slider and segments 1, 2, 3 and 4 are the distance the slider moves every 1.5 s. Then, according to the partitioning situation of the friction plane of the guide-ways, a mobile heat source loading method was presented, as shown in Fig. 5. Combined with the reciprocating motion of the table along the X-axis, the corresponding relationship between the friction heat generation and time was established. The total friction heat generated during the movement of the slider was separately loaded on the friction surfaces of the guide-ways.

Table 5 NCHTCs of the cylinder h_c (W m^{-2} K^{-1})

Ambient temperature	Wall temperature	Temperature difference	NCHTCs (h_c)	
			Theoretical values	Simulation values
11 °C	12 °C	1 °C	2.589	11.003
	13 °C	2 °C	3.078	13.082
	14 °C	3 °C	3.405	14.471
	15 °C	4 °C	3.656	15.538
	16 °C	5 °C	3.865	16.426
	17 °C	6 °C	4.043	17.183
	18 °C	7 °C	4.201	17.854
	19 °C	8 °C	4.341	18.449
	20 °C	9 °C	4.469	18.993
	21 °C	10 °C	4.586	19.491

Table 6 NCHTCs of the end face of the screw seat *hs* (W m^{-2} K^{-1})

Ambient temperature	Wall temperature	Temperature difference	NCHTCs (h_s)	
			Theoretical values	Simulation values
11 °C	12 °C	1 °C	2.631	11.182
	13 °C	2 °C	3.127	13.290
	14 °C	3 °C	3.459	14.701
	15 °C	4 °C	3.715	15.789

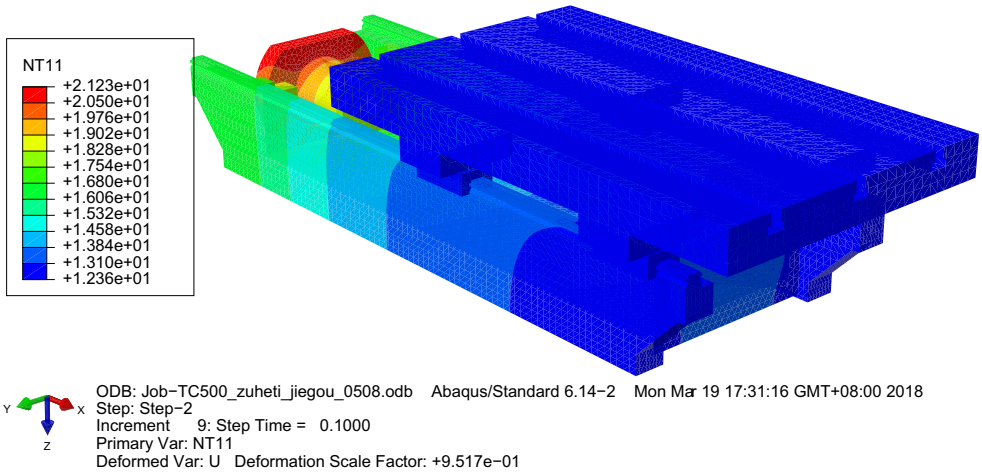

Fig. 7 Temperature distribution of the ball screw feed system

3.4.2 Calculation

For the machine tool ball screw feed system, the CHTC of the stationary part is the natural convection heat transfer coefficient (NCHTC). In this experiment, although the table was a moving part, its velocity was slow and uniform. The Reynolds number Re was used to determine that the table was still considered to be the NCHTC to compute. In addition, the physical parameters of the air were the same at the same temperature. When calculating the NCHTC of each part of the ball screw feed system, the NCHTC of the rectangular plane (plate) components with the same material were considered to be identical [26]. For cylindrical components, it was not possible to determine whether the size differences could be ignored; therefore, the differences were calculated separately in the text. Additionally, to improve the accuracy of the analysis, the NCHTC of the motor coupling surface of the rotating motor and NCHTC of the ball screw seat surface near the rotating ball screw were also separately calculated [27]. In summary, three NCHTCs were calculated, including

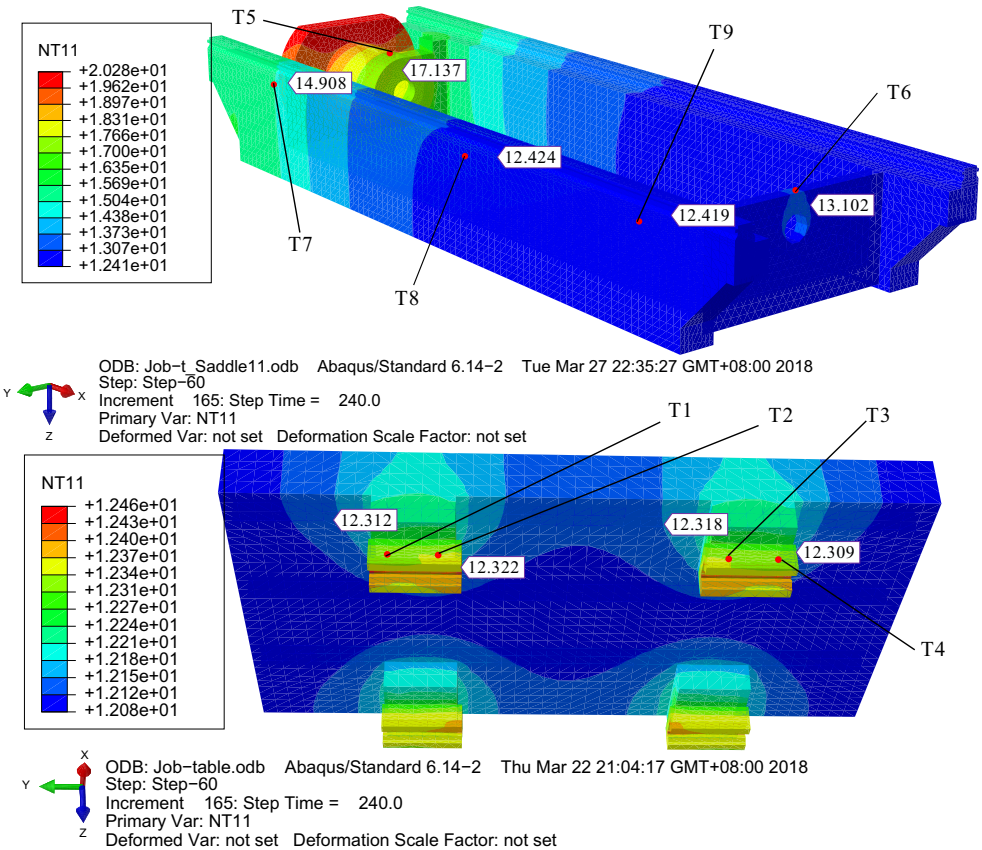

Fig. 8 Tradition simulation results of the temperature field

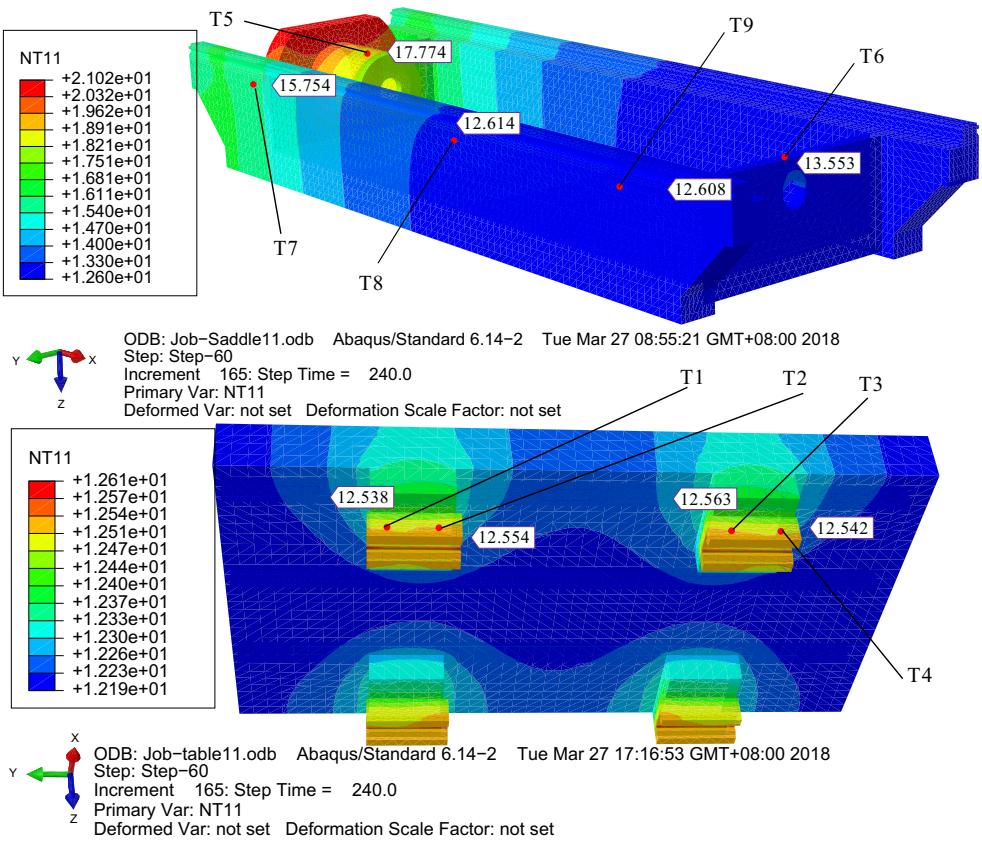

Fig. 9 Modified simulation results of the temperature field

the plate parts h_p, cylindrical parts h_c and end face of the ball screw seat h_s.

Dynamic setting of the CHTC was also a focus of this article. The inter-partition setting of CHTC was achieved with the help of ABAQUS and MATLAB. After setting the boundary conditions, the NCHTC was calculated by the method presented in this paper.

In the design experiment, after a short amount of assume time, the temperature difference was calculated by measuring the surface and initial ambient temperature of each component. Then, the program was called to calculate the initial NCHTCs of each component at that time, and through the cycle calculation, the final NCHTCs of each component were obtained. The exact simulation temperature field for the first 32 min is shown in Fig. 6 (with the temperature measurement points). During the entire experiment, the predicted total temperature difference was divided into multiple intervals, and the exact NCHTCs of each part were calculated according to the method presented in this paper. The calculated NCHTCs are shown in Tables 4, 5 and 6.

Finally, the best NCHTCs for each component were obtained; the program adopted these NCHTCs to perform a thermal

Table 7 Comparison of the temperature values and simulation errors

No. of the points	Simulated values (°C)		Experimental values (°C)	Simulation errors (%)	
	Tradition	Modified		Tradition	Modified
T1	12.312	12.539	12.690	−2.971	−1.189
T2	12.322	12.554	12.684	−2.854	−1.025
T3	12.318	12.563	12.706	−3.053	−1.125
T4	12.309	12.547	12.689	−3.071	−1.119
T5	17.137	17.974	18.087	−5.252	−0.625
T6	13.102	13.353	13.675	−4.190	−2.354
T7	14.895	15.754	16.015	−7.685	−1.629
T8	12.424	12.614	12.688	−2.081	−0.583
T9	12.419	12.608	12.572	−1.217	0.286

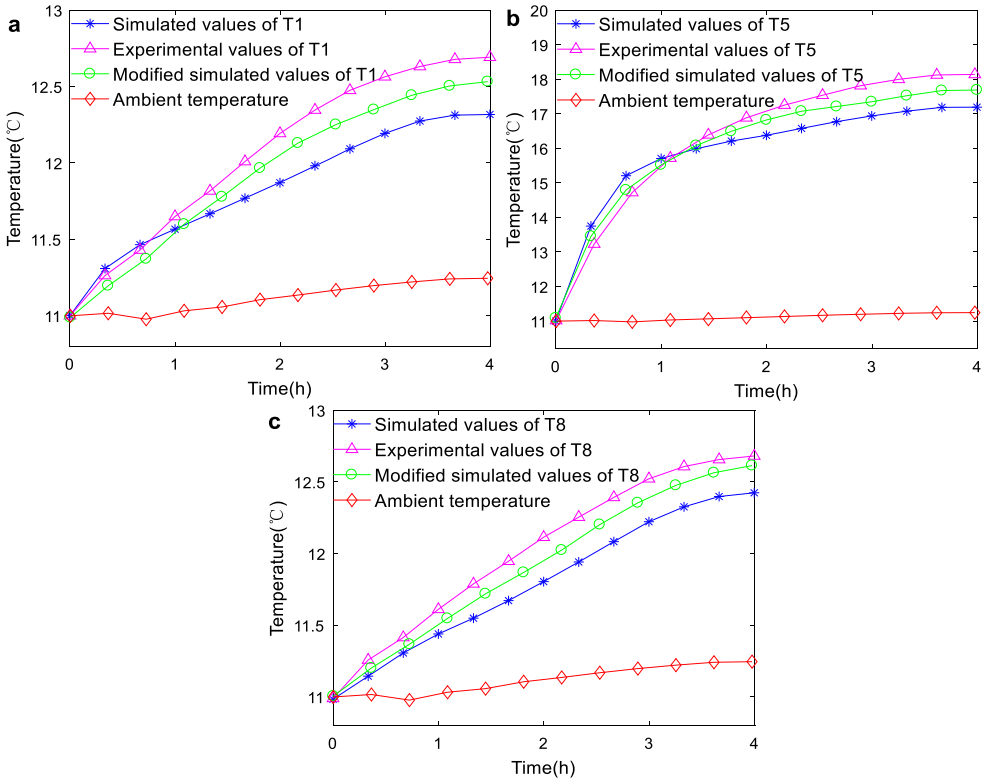

Fig. 10 Comparison of the temperature values

analysis of the entire ball screw feed system of the machine tool. The final calculated temperature field is shown in Fig. 7.

3.5 Calculation results

From the above calculations, it is observed that the NCHTC gaps in different temperature ranges were relatively large. Particularly when the object temperature was high, the NCHTC of a large temperature difference even reached 2–3 times that of the NCHTC under a small temperature difference. Hence, it was necessary to segment the NCHTC. To further illustrate the advantage of the proposed calculation method, the simulation results by the method presented in this paper were compared with simulation results calculated by the traditional empirical formula. The simulated temperature field and the modified simulation temperature field are shown in Fig. 8 and Fig. 9, respectively. Meanwhile, two types of simulation errors were calculated, as shown in Table 7. Otherwise, the simulated and measured temperature values of T1, T5 and T8, which were larger temperature differences and distributed on different components, were compared. The temperature curves of the three points were plotted, as shown in Fig. 10.

By analysing the calculation results, it was observed that the iterative computation method proposed in this paper was not only accurate but also improved precision compared with the traditional experience method. Particularly at a relatively high temperature, the simulation results were closer to the experimental results. Furthermore, the biggest advantage of the algorithm presented in this paper was that it was relatively easy to measure only a few points and the exact CHTCs could be calculated using a FE thermal simulation and the experimental data. Using these CHTCs, the accurate temperature field distribution of the object was determined.

Table 8 NCHTCs h_c at different ambient temperatures (W m^{-2} K^{-1})

Temperature	h_c1	h_c2	h_c3	h_c4	h_c5	h_c6	h_c7	h_c8	h_c9	h_c10
15 °C	10.97	13.03	14.42	15.49	16.36	17.12	17.79	18.38	18.93	19.42
17 °C	10.94	13.01	14.39	15.46	16.34	17.09	17.76	18.35	18.89	19.38
21 °C	10.90	12.96	14.34	15.40	16.28	17.03	17.69	18.28	18.82	19.32
24 °C	10.87	12.93	14.29	15.36	16.23	16.98	17.64	18.24	18.77	19.27
27 °C	10.84	12.89	14.26	15.32	16.19	16.94	17.59	18.19	18.72	19.21
30 °C	10.81	12.85	14.22	15.27	16.14	16.91	17.55	18.13	18.67	19.16

Table 9 NCHTCs h_p at different ambient temperatures (W m^{-2} K^{-1})

Temperature	h_p1	h_p2	h_p3	h_p4	h_p5	h_p6	h_p7
15 °C	7.42	8.82	9.76	10.48	11.08	11.59	12.04
17 °C	7.41	8.81	9.74	10.46	11.06	11.58	12.03
21 °C	7.38	8.77	9.70	10.42	11.02	11.53	11.97
24 °C	7.36	8.75	9.68	10.39	10.99	11.50	11.94
27 °C	7.34	8.73	9.65	10.37	10.96	11.46	11.91
30 °C	7.32	8.70	9.63	10.34	10.93	11.43	11.88

Table 10 NCHTCs hs at different ambient temperatures (W m^{-2} K^{-1})

Temperature	h_s1	h_s2	h_s3	h_s4	h_s5
15 °C	11.14	13.24	14.65	15.73	16.63
17 °C	11.12	13.22	14.62	15.71	16.60
21 °C	11.08	13.17	14.57	15.65	16.54
24 °C	11.05	13.13	14.53	15.61	16.49
27 °C	11.02	13.10	14.49	15.56	16.45
30 °C	10.98	13.06	14.45	15.52	16.40

4 Relationship between ambient temperature and the NCHTC

4.1 Verification of the NCHTC at different ambient temperatures

The NCHTC was affected by ambient temperature changes; therefore, the environmental temperature should be considered when calculating the NCHTC. On the basis of the NCHTC calculation method described above, multiple experiments at different temperatures over 1 year were conducted to study the specific impact of ambient temperature changes on NCHTC. Six groups of experiments at different temperatures were selected to illustrate the process and detail the results, and the relationship between the NCHTC and temperature was provided.

Since the temperature range of the workshop was approximately 10–30 °C in 1 year, according to the actual condition of the workshop, the ambient temperatures of the six experimental groups were 15, 17, 21, 24, 27 and 30 °C. According to the prediction highest temperature, the temperature differences of the plate parts, cylindrical parts and end face of the

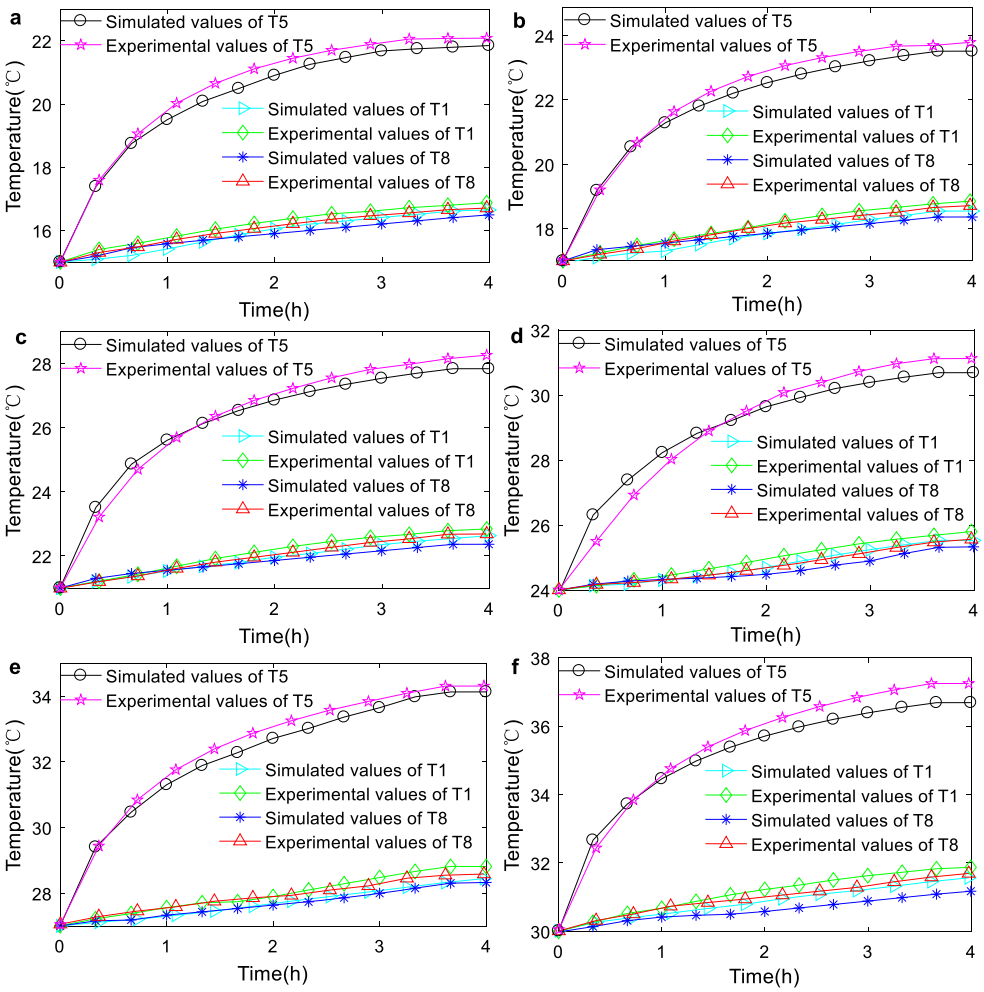

Fig. 11 Comparison of the temperature values of the six groups

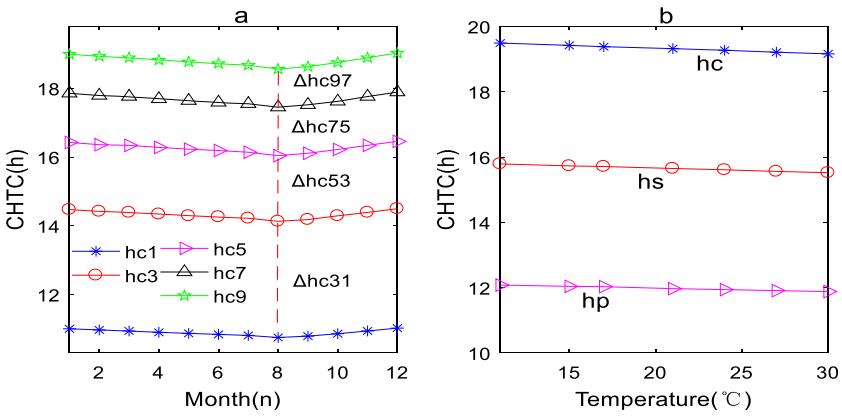

Fig. 12 Variation situation of NCHTC within 1 year

ball screw seat were divided into 10 intervals, 7 intervals and 5 intervals, respectively. The initial temperature difference was 1 °C, and the temperature difference was increased by 1 °C. Then, the homologous NCHTCs of each interval were computed, as shown in Tables 8, 9 and 10.

Three measuring points, T1, T5 and T8, were also chosen, and the simulation results of above six groups were compared with the experimental values, as shown in Fig. 11.

4.2 Results and discussion

The temperature changes over 1 year of studying machine tool's location showed a gradually increasing trend from January to August, but the trend decreased after August. Through the simulation and an experimental comparison of the six groups described above, it was observed that the proposed dynamic thermal boundary loading mode and calculation method of the NCHTC were feasible and accurate. Meanwhile, the greater the temperature increase, the greater the NCHTC required for thermal analysis. The component movement can drive the airflow, which increases the NCHTC. The specific relationship between the NCHTC and temperature is summarised as follows: (1) at the same temperature difference Δt, the NCHTC gradually decreased with the increase of the ambient temperature, as shown by the left red dotted line in Fig. 12a. (2) Under the same ambient temperature, as the temperature difference Δt increased, the magnitude of the NCHTC increase slowed, as shown by the dashed red line in Fig. 12a. Under a thermal steady state, the variation situation of three NCHTC values, h_p, h_c and hs, with the temperature is as shown in Fig. 12b.

However, according to the traditional similar principle, the NCHTC of the same material should be the same under the same temperature difference. Nevertheless, the NCHTC changes when considering the variety of ambient temperatures. Therefore, the above experimental phenomena were analysed and explained below.

The physical parameters of air vary when the ambient temperature increases, leading to changes in the NCHTC. The dynamic viscosity, density, kinematic viscosity and thermal diffusivity were the main parameters that caused changes in the NCHTC. Other factors, such as the specific heat capacity, thermal conductivity and Prandtl number (Pr) showed little effect. It was found that the most influential parameter was the kinematic viscosity, followed by the dynamic viscosity and, finally, the thermal diffusivity. Moreover, with the temperature increases, these parameters gradually increased; however, the specific qualitative relationship between them and the NCHTC requires further study.

5 Conclusions

In this paper, a cyclic iterative calculation method of CHTC based on experimental data and FE thermal analysis was proposed. Experimental values were introduced at the beginning of the iterative computation, and the calculation accuracy was improved by cycling. In addition, taking into account the effect of temperature changes in the calculation process, the dynamic mode of the CHTC setting was given by thinning the temperature difference. The proposed method has the following advantages: (1) it is simple and operable. (2) In the initial stage of the simulation, a judgement can be made by comparing the simulation results with experimental values. Therefore, this judgement could play a predictive role and reduce the computation time and computation cost. (3) The experimental data are added to the cyclic iterative calculation to ensure the calculation accuracy. (4) The dynamic CHTC setting mode is closer to the actual situation, and the simulation credibility is higher.

Additionally, this article reveals the relationship between the NCHTC and ambient temperature. The refinement of the temperature difference was able to successfully calibrate the NCHTC, which provides a new idea and reference for the calculation and setting of the CHTC, especially for simulations and analyses of objects with large temperature differences and time consumption.

Nevertheless, the study presented in this paper was only on a machine tool ball screw feed system. Future work should investigate the improvement of thermal the simulation accuracy of machine tools.

Funding This work is supported by the National High Technology Research and Development Program of China (863 Program) by the grant no. 2015AA043302.

References

1. Jędrzejewski J, Kaczmarek J, Kowal Z, Winiarski Z (1990) Numerical optimization of thermal behaviour of machine tools. CIRP Ann Manuf Technol 39(1):379–382
2. Lee JH, Yang SH (2002) Statistical optimization and assessment of a thermal error model for CNC machine tools. Int J Mach Tool Manu 42(1):147–155
3. Han J, Wang L, Wang H, Cheng N (2011) A new thermal error modeling method for CNC machine tools. Int J Adv Manuf Technol 62(1–4):205–212
4. Mayr J, Jedrzejewski J, Uhlmann E, Donmez MA, Knapp W, Hartig F, Wendt K, Moriwaki T, Shore P, Schmitt R, Brecher C, Wurz T, Wegener K (2012) Thermal issues in machine tools. CIRP Ann Manuf Technol 61(2):771–791
5. Babaelahi M, Sayyaadi H (2015) A new thermal model based on polytropic numerical simulation of Stirling engines. Appl Energy 141(1):143–159
6. Vyroubal J (2012) Compensation of machine tool thermal deformation in spindle axis direction based on decomposition method. Precis Eng 36(1):121–127
7. Zhao HT, Yang JG, Shen JH (2007) Simulation of thermal behavior of a CNC machine tool spindle. Int J Mach Tool Manu 47(6):1003–1010
8. Lee S (2011) An experimental apparatus measuring convective heat transfer coefficient from a heated fine wire traversing in nanofluids. J Mech Sci Technol 25(1):135–142
9. Weck M, McKeown P, Bonse R, Herbst U (1995) Reduction and compensation of thermal errors in machine tools. CIRP Ann Manuf Technol 44(2):589–598
10. Yang H, Yin GF, Fang H, Liu LX, Zhang DJ, Xu DW (2013) Research on calculation methods of convective heat transfer coefficients for machine tools' thermal analysis. J Sichuan Univ (engineering science edition) (in Chinese) 43(4):241–248
11. Li DX, Feng PF, Zhang JF, Wu ZJ, Yu DW (2014) Calculation method of convective heat transfer coefficients for thermal simulation of a spindle system based on RBF neural network. Int J Adv Manuf Technol 70(5–8):1445–1454
12. Fang CL, Sun FR, Yang L (2008) A numerical method on inverse determination of heat transfer coefficient based on thermographic temperature measurement. Chin J Chem Eng 16(6):901–908
13. Zhang JF, Feng PF, Chen C, Yu DW, Wu ZJ (2013) A method for thermal performance modeling and simulation of machine tools. Int J Adv Manuf Technol 68(5–8):1517–1527
14. Shi H, Zhang D, Yang J, Ma C, Mei X, Gong G (2015) Experiment-based thermal error modeling method for dual ball screw feed system of precision machine tool. Int J Adv Manuf Technol 82(9–12):1693–1705
15. Neugebauer R, Ihlenfeldt S, Zwingenberger C (2010) An extended procedure for convective boundary conditions on transient thermal simulations of machine tools. Prod Eng 4(6):641–646
16. Xu Z-Z, Choi C, L-j L, Li D-y, Lyu S-K (2015) Study on a novel thermal error compensation system for high-precision ball screw feed drive (2nd report: experimental verification). Int J Precis Eng Manuf 16(10):2139–2145
17. Awbi HB (1998) Calculation of convective heat transfer coefficients of room surfaces for natural convection. Energy and Buildings 28:219–227
18. Miao EM, Liu Y, Liu H, Gao ZH, Li W (2015) Study on the effects of changes in temperature-sensitive points on thermal error compensation model for CNC machine tool. Int J Mach Tool Manu 97:50–59
19. Miao EM, Gong YY, Dang LC, Miao JC (2014) Temperature-sensitive point selection of thermal error model of CNC machining center. Int J Adv Manuf Technol 74(5–8):681–691
20. Lou P, Liu NY, Chen YT, Liu Q, Zhou ZD (2017) The selection of key temperature measuring points for the compensation of thermal errors of CNC machining tools. Int J Manuf Res 12(3):338–350
21. Wu CH, Kung YT (2003) Thermal analysis for the feed drive system of a CNC machine center. Int J Mach Tool Manu 43(15):1521–1528
22. Kim JJ, Jeong YH, Cho DW (2004) Thermal behavior of a machine tool equipped with linear motors. Int J Mach Tool Manu 44(7–8):749–758
23. Xu M, Jiang SY, Cai Y (2007) An improved thermal model for machine tool bearings. Int J Mach Tool Manu 47(1):53–62
24. Lin B, Morgan MN, Chen XW, Wang YK (2008) Study on the convection heat transfer coefficient of coolant and the maximum temperature in the grinding process. Int J Adv Manuf Technol 42(11–12):1175–1186
25. Ma SJ, Liu G, Qiao G, Fu XJ (2015) Thermo-mechanical model and thermal analysis of hollow cylinder planetary roller screw mechanism. Mechanics Based Design of Structures and Machines 43(3):359–381
26. Costa SF, Duarte FM, Covas JA (2014) Thermal conditions affecting heat transfer in FDM/FFE: a contribution towards the numerical modelling of the process. Virtual and Physical Prototyping 10(1):35–46
27. Yun WS, Kim SK, Cho DW (1999) Thermal error analysis for a CNC lathe feed drive system. Int J Mach Tool Manu 39(7):1087–1101